Hardware Development for the Surface Tension Driven Convection Experiment

A. D. Pline,* T. P. Jacobson,† J. S. Wanhainen,‡ and D. A. Petrarca‡
NASA Lewis Research Center, Cleveland, Ohio, 44135

The Surface Tension Driven Convection Experiment is a Space Transportation System flight experiment to study both transient and steady thermocapillary fluid flows aboard the USML-1 Spacelab mission planned for March 1992. Hardware is under development to establish the experimental conditions and to perform the specified measurements for both ground-based research and the flight experiment in a Spacelab single rack. Major development areas include an infrared thermal imaging system for surface temperature measurement, a CO_2 laser and control system for surface heating, and, for flow visualization, a He-Ne laser and optical system in conjunction with an intensifed video camera. For ground-based work, the components of each system have been individually purchased or designed and tested. The three systems will be interfaced with the balance of the experimental hardware and will constitute a working engineering model.

Introduction

ACCESS to the low-gravity environment aboard the Space Transportation System (STS), or Space Shuttle, offers unique opportunities for both scientific research and commercial ventures. For example, containerless processing of materials aboard the STS is possible because of the extended duration of low gravity. Because the effects of natural convection are minimized and contact with a processing crucible may be eliminated in this environment (two of the main sources of imperfections in terrestrial materials processing), the possibility of growing better quality crystals by containerless methods is becoming a reality.

Because liquid/gas-free surfaces are inherent to containerless processes, surface-tension driven flows in reduced gravity become significant.[1] Surface tension driven flows, or thermocapillary flows are driven by a thermally induced, surface-tension variation along a liquid-gas free surface. This surface tension gradient, established by heating the surface, is a surface-tractive force, which creates a flow parallel to the liquid-gas free surface from regions of low-surface tension to high-surface tension. Under certain conditions thermocapillary flow becomes oscillatory[2] and may detrimentally affect the growth of crystals. Therefore, an understanding of the basic science of both steady-state and oscillatory thermocapillary flow is needed in order to realize any benefit from low-gravity materials processing.

As discussed by Ostrach and Kamotani,[3,4] thermocapillary flows, both steady state and oscillatory, have been demonstrated in space.[5,6] To study these phenomena in a more quantitative fashion, Kamotani and Ostrach[3] described the considerations and parameters that influence the design of a thermocapillary flow experiment in reduced gravity, resulting in the design of the Surface Tension Driven Convection Experiment (STDCE).

This paper describes the development of three major systems that will be used to establish the experimental conditions and to perform some of the desired measurements: an infrared imaging system to measure fluid surface temperatures, a CO_2 laser and control system for surface heating, and a He-Ne laser and optical system in conjunction with an intensified video camera for flow visualization. These major systems will be integrated with other systems and will comprise a working engineering model of the experiment. At the present time, plans are in progress to procure flight versions of these four components; all other hardware is under design at the NASA Lewis Research Center.

Overview of Surface Tension Driven Convection Experiment

The two experimental configurations for the STDCE are illustrated in Fig. 1: a constant temperature boundary condition (called CT experiment) and a constant flux boundary condition (called CF experiment). Two configurations are studied for several reasons. In the CT experiment, the total temperature difference along the free surface is imposed by heating and cooling opposing walls. This temperature difference is related to the magnitude of the driving force[7] and can be directly measured. In the CF experiment, various heat flux distributions are imposed along the free surface using a radiant heater as the effect of the distributions on the flow is studied.[8]

Both experimental configurations use a cylindrical container of 10 cm in diameter and 5 cm in height. The STDCE is conducted in two discrete segments. For the CT experiment a 1.1-cm-diam × 5-cm-high resistance heater (heated wall) is placed in the center of the test cell (cooled wall). For the CF experiment, the resistance heater is removed and the free surface is heated using a radiant heater. For both CT and CF experiments, the test container is filled to different levels to create both flat and curved free surfaces. Because the thermocapillary driving force acts tangentially to the local free surface, variations in free surface shape permit different driving forces to be used as an experimental parameter. A flat, free surface greatly simplifies both the theoretical and experimental analyses and therefore will be used for most of the experiments. A curved free surface, which is unique to a low gravity environment, allows the investigation of a driving force, which cannot be studied in a terrestrial environment. Consequently, verification of experimental techniques described herein in conjunction with a curved free surface, is not included in the present work. Test matrices, which include temperature gradient ΔT, Marangoni number[7] Ma, heater power, free-surface shape, and duration for both CT and CF experiments are presented in Tables 1 and 2. A more detailed explanation of other experimental considerations and parameters is given in the literature.[1,3,6,7]

Presented as paper 89-0406 at the AIAA 27th Aerospace Sciences Meeting, Reno, NV, Jan. 9-12, 1989; received Jan. 26, 1989; revision received Aug. 23, 1989.

*Surface Tension Driven Convection Experiment (STDCE) Research Engineer, Space Experiments Division. Member AIAA.
†STDCE Project Manager, Space Experiments Division.
‡STDCE System Engineer, Engineering Directorate.

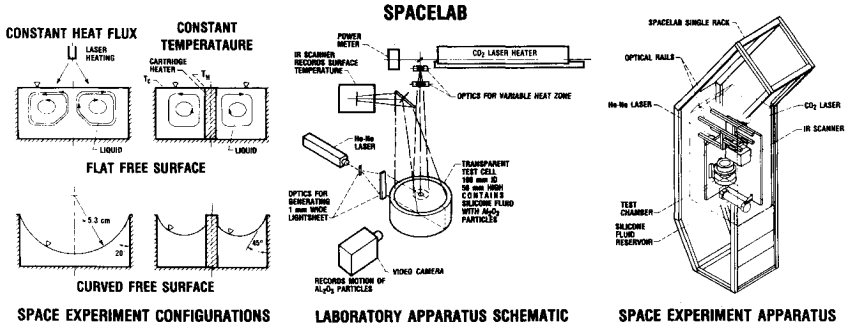

Fig. 1 Surface Tension Driven Convection Experiment.

Table 1 Constant flux tests

Test No.	Heating zone diam, mm	Total power W	ΔT, °C	Ma[a]	Surface shape[b]	Duration, min
1	10	0.5	10.4	4.2×10^4	flat	60
2	10	3.0	36.8	1.5×10^5	flat	10
3	30	3.0	12.4	5.0×10^4	flat	10
4	5	0.2	10.2	4.1×10^4	flat	10
5	5	3.0	64.7	4.4×10^5	flat	10
6	5	3.0	$\approx$64.7	$\approx2.2\times10^5$	curved	10
7	30	3.0	$\approx$12.4	$\approx2.5\times10^4$	curved	10

[a]Ma is based on average liquid depth. [b]Values of ΔT and Ma for the flat surface tests are computed by numerical analysis; those for the curved surface tests are estimates.

Table 2 Constant temperature tests

Test No.	Heater power, W	ΔT, °C	Ma[a]	Surface shape[b]	Duration, min
8	1.5	10	3.9×10^4	flat	60
9	6.8	25	1.2×10^5	flat	10
10	32.8	60	4.1×10^5	flat	10
11	$\approx$1.5	10	$\approx3.2\times10^4$	curved	10
12	$\approx$32.8	60	$\approx3.3\times10^5$	curved	10

[a]Ma is based on average liquid depth. [b]Values of heater power for the flat surface tests are computed numerically; those for the curved surface tests are estimates.

The experimental hardware for the STDCE is currently in a design phase. The test chamber is made of copper to insure good thermal boundary conditions at the side wall. A 10-cSt silicone oil is used as the test fluid because it is insensitive to surface contamination (a common problem with surface tension experiments), it is safe, and its viscosity represents the best compromise between flow speed and susceptibility to free surface disturbances. A planar cross section is illuminated using a 1-mm-wide He-Ne laser light sheet, which is reflected by seed particles in the fluid allowing observation of the flows. Because this geometry produces an axisymmetric flow, illumination of only one cross section is needed. The flow data are observed using an intensified video camera, which views the light sheet through a view port in the copper chamber, and are recorded using a video cassette recorder for a postflight analysis. Bulk flow temperatures are measured using temperature probes placed in the fluid. The heating systems used are a resistance heater (CT experiment) and a CO_2 laser (CF experiment). A thermographic technique is used to measure the surface temperature. The imager output is also recorded on videotape, and temperature distributions are determined from the thermographs after flight. This hardware is configured to occupy the lower half of a spacelab double rack.

Science Requirements

The hardware described in this paper was developed in response to the science requirements developed by the Principal and Co-investigator (S. Ostrach and Y. Kamotani of Case Western Reserve University). These requirements are necessary to define and guide the development of the experimental hardware. An outline of the requirements for the systems described herein is presented here; the requirements for the experiment in its entirety are given in Ref. 8.

Surface Temperature Measurement

The requirements for the surface temperature measurement system are for a full-field nonintrusive measurement using a thermographic technique. The operational wavelength should be chosen so that the detected radiation comes from a region as close to the surface as possible. The spatial resolution and response time should be $\leq$ 1mm and 0.1 s, respectively. The accuracy of the instrument should be with $\pm5\%$ of the ΔT between the center and side wall. To satisfy these requirements, the technique should be calibrated against measurement by fine thermocouples as well as numerical analysis.[8]

Surface Heating System

For the CF experiments, a remote heat source is required. To obtain effective surface heating and to simulate heating of an opaque liquid metal in crystal growth (processes), it is desirable that the radiation be absorbed within a small distance from the surface ($\sim$1 mm).[8] The accuracy of the output power should be $\pm10\%$ of the specified value and the fluctuations in time limited to $\pm5\%$ with a warm up time of $<$1 min.

Flow Visualization

The requirements for two-dimensional flow visualization are for a 1-mm light sheet to illuminate aluminum oxide particles in a full cross section of the test chamber. The particles should be 1–20 μm in size with an optimum concentration. The camera and recording device should have a spatial resolution of 0.2 mm.

System Design and Performance

Surface Temperature Measurement System

The analyses by Ostrach and Kamotani[3,7] identified the thermal signature along the free surface as a critical parameter, as it is the driving force for thermocapillary flows. Therefore, quantification of the thermal signature is essential for both ground-based research and the flight experiment. This is accomplished using an infrared thermal imaging system (Fig. 2) to perform the measurements in the laboratory. The performance of this system is used as a baseline for a flight qualified version.

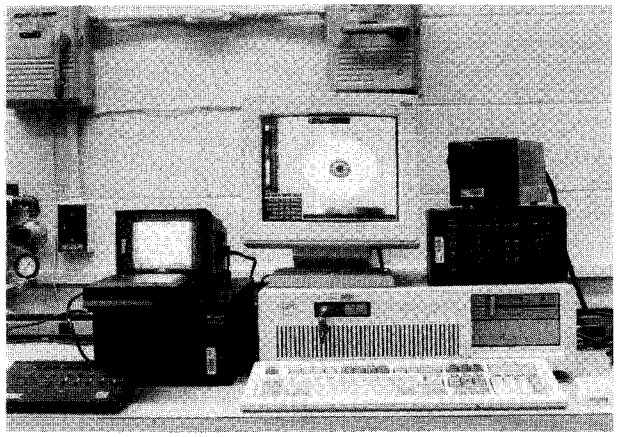

Fig. 2 Infrared thermal imagining system.

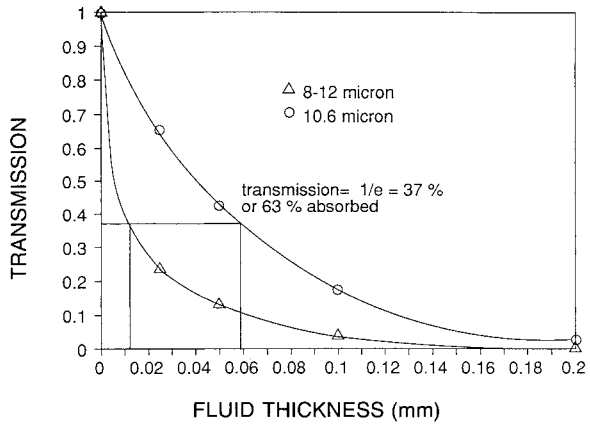

Fig. 3 Transmission vs fluid thickness: mean absorption lengths.

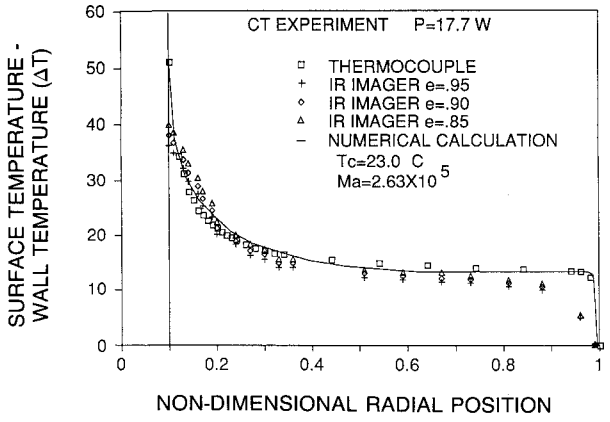

Fig. 4 Empirical determination of effective emissivity.

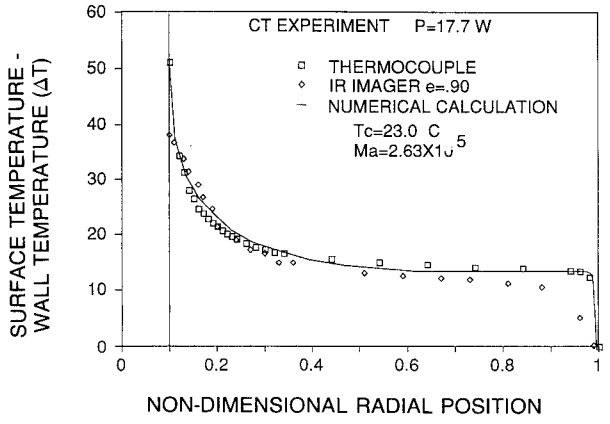

Fig. 5 Surface temperature distributions: CT experiment.

In his work with this system, Pline[9] details the step-by-step process undertaken to understand and calibrate the infrared imager for this application as outlined in Ref. 8. The considerations examined for this system were the absorption characteristics of silicone oil, effective emissivity of silicone oil, and the agreement of the imager measurements with thermocouple measurements and numerical calculations.

Absorption Length

The absorption characteristics of silicone oil must be known to understand the thickness of the "surface" as seen by the imager. For semitransparent targets, radiation is emitted (absorbed) over varying depths depending on the radiation wavelength and material properties. If this depth, usually referred to as the mean absorption length, $1/k$, where k is the extinction coefficient, is much less than the total fluid thickness, the material is said to be opaque. As a result, the measurement of the emitted radiation is considered to be from the surface. Physically, the mean absorption length represents the fluid thickness, which attenuates the incident radiation by a factor of $1/e$ (37% transmitted or 63% absorbed).

Results for the mean absorption length for the spectral region, corresponding to the operating wavelength region of the imager, were obtained using a infrared spectrophotometer. The spectrophotometer measures radiation attenuated through a variable thickness of fluid as a function of wavelength. The transmission vs wavelength results show that silicone oil is very transparent under 8 μm. Therefore, an imager that operates in the far infrared (>8 μm) is needed. To find the mean absorption length, the transmission through the fluid is averaged over the operating wavelength of the imager (8-12 μm) and plotted against fluid thickness (Fig. 3). The mean absorption length is found graphically from this plot to be 0.012 mm. Also, the fluid thickness which attenuates nearly 100% of the incoming radiation is found to be 0.200 mm. From these results, it is concluded that the surface the imager sees is 0.200-mm thick.

Effective Emissivity

Because no surface is an ideal radiator, here is an emissivity (<1) associated with the surface. This emissivity is needed as an input to the thermal imaging system to account for nonblack and reflected background radiation. There is no existing literature documenting the emissivity of silicone oil. Thus, an emissivity is determined empirically. This value is called the effective emissivity because it is implied by comparison of the imager surface temperature data with other techniques, rather than by direct measurement.

Temperature distributions from thermocouples and numerical calculations are compared to temperature distributions from the imager using different values of the emissivity. From this comparison, surface temperature difference $T-T_c$, where T_c is the cooled wall temperature, is plotted against nondimensional radial position r/R, where R is the radius of the test chamber. The emissivity value of 0.90 gives the best agreement with the thermocouple measurements and the calculated surface temperature (Fig. 4). It must be noted that this effective emissivity measurement is specific to this imaging system and these experimental conditions.

Accuracy

Data acquired using the infrared imaging system for both the CT and CF experiments are analyzed and compared to thermocouple measurements and a calculated surface temperature distribution to establish the accuracy of the system.

Shown in Fig. 5 is the comparison of the three techniques for the maximum temperature gradient expected for the CT experiment (test 10, Table 2), which is the most difficult CT

measurement case. The agreement between the techniques for this case (and a lower power case not shown) is ±5% of the overall ΔT between the heater and the side wall in all but the regions close to the walls. These errors near the walls are caused by several factors including the imager spatial resolution, low surface emissivity of the wall, and a meniscus at the wall. These sources of errors and their possible solutions are discussed elsewhere in detail.[9]

The results shown in Fig. 6 are for the most difficult CF measurement case (test 5, Table 1). The accuracy as compared to the numerical calculation is ±5% of the ΔT except near the wall and in the center of the heating zone. Only the numerical analysis was used for the comparison because thermocouple measurements could not be made with any certainty due to the thin thermal boundary layer under the heating zone and the effect of direct heating of the thermocouple by the CO_2 laser. As with the CT experiment, the measurement errors increased near the side wall for reasons stated previously. Near the center, the errors increased because of the aforementioned boundary-layer thickness. The imager reports a lower temperature than the numerical calculation because the imager "sees" through the boundary layer and detects radiation from the cooler fluid beneath the thermal boundary layer.

The plans for obtaining a flight-qualified infrared imager are in progress. An imager will be developed, fabricated, tested, and qualified for flight. The completion date for the flight version will correspond with the fabrication and integration of all hardware into the complete flight configuration.

Surface Heating System

Several requirements have driven the surface heating system design towards a remote radiant heater for the CF experiments. It is necessary to change the radiation signature of the heater for the different test runs, and it is desirable, from safety considerations, to locate the source of the radiation away from the free surface. A radio frequency (rf) exited waveguide CO_2 laser (Fig. 7), shown with a piggy back low power He-Ne laser used for alignment in the laboratory, was chosen as the surface heater for several reasons. It produces radiation at a wavelength, which silicone oil readily absorbs (10.6 μm). The beam diameter is easily varied through a combination of lenses, and it can be controlled to produce a steady output. These features facilitate meeting the science requirements.

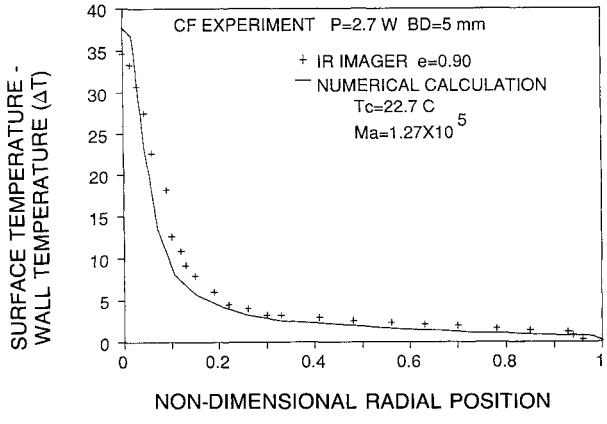

Fig. 6 Surface temperature distributions: CF experiment.

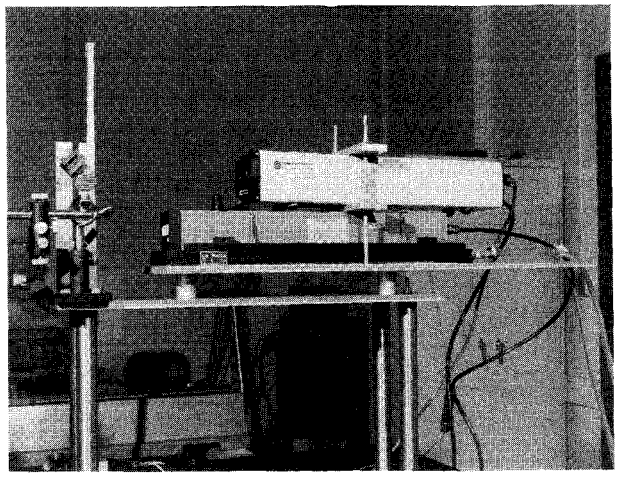

Fig. 7 CO_2 laser.

Absorption Length

In addition to the 8–12 μm region absorption length, an absorption length for the CO_2 laser radiation was calculated at 10.6 μm. Transmission at 10.6 μm was plotted vs fluid thickness (see Fig. 3). From this figure the mean absorption length is 0.060 mm. The fact that the CO_2 laser radiation penetrates deeper than the imager sees is advantageous because, if the situation is opposite, the temperature indicated by the imager is an average over a region where a large temperature gradient exists.

Power Control System Design

To remove waste heat, the CO_2 laser is mounted on a water-cooled base plate, which removes the heat via conduction. The stability of the output power (both wavelength and amplitude) is dependent on the thermal stability of the laser and will, therefore, be a function of the thermal stability of the base plate. In the laboratory, the output power fluctuations measured with the present laser without a closed-loop control system can be held to within the science requirements by circulating tap water through the base plate. Operation aboard the Shuttle is considerably different due to the temperature fluctuations in the open-loop Spacelab cooling system. Open loop control tests indicate the fluctuations with time, under Spacelab simulated conditions, exceed that allowed by the science requirements. Therefore, an active control system was designed by Wenzler and Eichenberg[10] to control the laser output.

A block diagram of the basic design is shown in Fig. 8. The principle of the design is that the laser output is controlled and varied over a small range (3–4 W) using a closed-loop system. The different power levels required (see Table 1) are created using variable ratio beam splitters as turning mirrors to deflect the desired amount of radiation to the free surface. Small changes in set point will be required to compensate for any errors in the beam splitter ratios. The closed loop operates in the following manner: a set point is entered into a PID controller from the STD bus (the onboard experiment computer), and a control signal, called the trim voltage, is fed to a dc-dc, power converter, which draws power from the Spacelab power bus. The converter has a gate, which is essentially a switch that

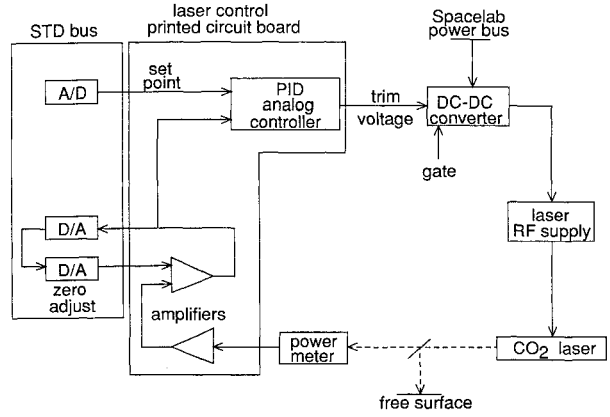

Fig. 8 CO_2 laser, closed-loop, control system block diagram.

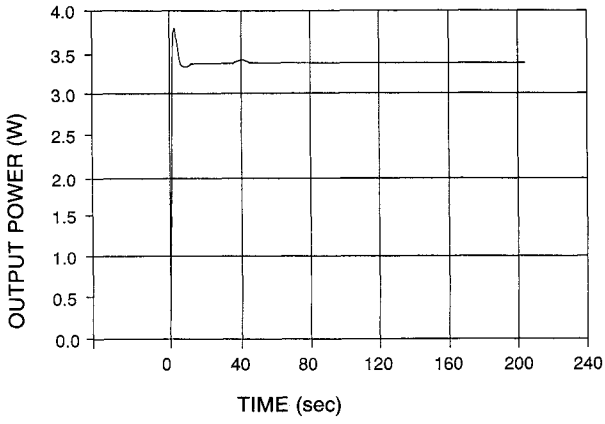

Fig. 9 CO_2 laser output vs time with closed-loop control.

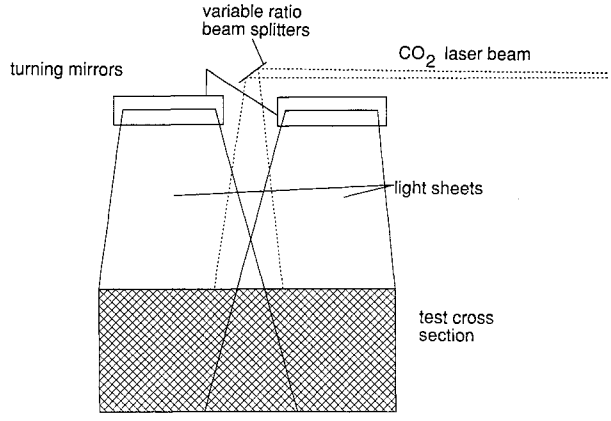

Fig. 11 Side view of optical path.

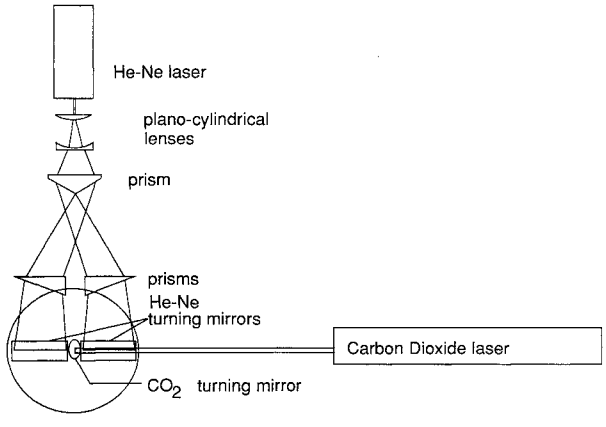

Fig. 10 Top view of optical path.

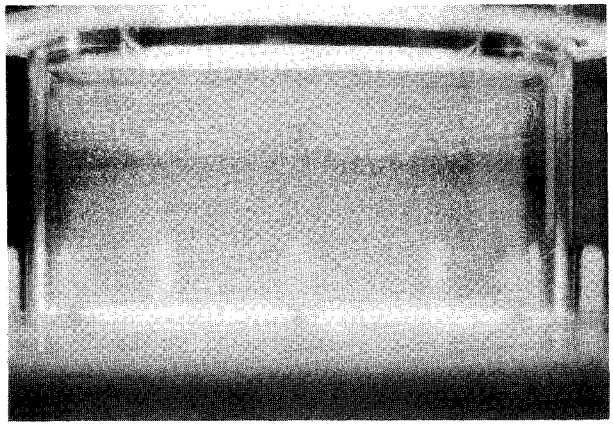

Fig. 12 STDCE CF experiment flow structure.

opens and closes the circuit to start and stop the laser operation. The output of the converter is proportional to the trim voltage regardless of the Spacelab power bus fluctuations. This voltage powers the CO_2 laser rf power supply and in turn regulates the output power of the laser. As mentioned previously, the laser beam is split to the desired ratio with the fraction not reaching the surface entering a power meter. The power meter output is input to the laser control printed circuit board and is amplified. A provision for adjusting the zero reading is added by measuring the signal with the gate open and nulling it via the STD bus. The signal is then input to the controller, compared to the set point and adjusted accordingly, completing the loop.

Test Results

Both the open-loop and closed-loop control systems have been tested extensively. As already mentioned, the output power fluctuations using the open-loop control are with the science requirements (good thermal control) and exceed the science requirements (no thermal control). The closed-loop control results show that this system is more than adequate to meet the science requirements. Figure 9 is a typical plot of the laser output as a function of time, beginning from startup. Power is within $\pm 2\%$ of the set point after 10 s. Tests were run to determine the effects of Spacelab power bus and cooling loop fluctuations. In all cases simulating the Spacelab conditions, the output power was similar to that in Fig. 9. The system must be calibrated with the optical components in place (lenses, beam spitters, windows, etc.) in order to determine accurately the setpoint voltages.

Similar to the IR imager, a CO_2 laser will be designed, fabricated, tested, and qualified for flight aboard the Shuttle.

Flow Visualization System

The second major type of data to be returned with the STDCE is a record of the fluid motion. The two main components of this system are a low-power He-Ne laser and an intensified video camera. The basic concept, outlined previously, is to expand a He-Ne laser into a sheet of small thickness and to illuminate a cross section of the test chamber. Aluminum oxide particles mixed in the fluid reflect the He-Ne light, which is received by the video camera. This signal is then recorded on a video cassette recorder for later analysis.

Design Considerations

Several factors contributed to the present design; for example, power consumption of the He-Ne laser vs light levels for the video camera and optical paths of the He-Ne and CO_2 laser beams. A major consideration for a Shuttle flight experiment is power consumption. In order to keep the power consumption low, a 5 mW, He-Ne laser drawing approximately 20 W was selcted as an illumination source. If the flow is to be observed using such a low-power source, an intensified video camera is needed to detect enough light to produce a usable image regardless of particle concentration (within the ranges practical for this application). The camera now in use in the laboratory is a silicon intensified tube (SIT) camera. The resolution of this camera is approximately 700 TV lines at light levels of 10^{-2} to 10^{-3} lux providing a spatial resolution better than 0.2 mm. This resolution is above what is needed because the recording technique used (S-VHS in the laboratory and 3/4 in. on the Spacelab) has the limiting resolution of approximately 400 TV lines, which reduces the resolution to approximately 0.25 mm. The combination of these two pieces of equipment produces suitable standard TV images for a

postflight analysis. The second consideration is the optical paths of the CO_2 and He-Ne lasers. In order to illuminate a cross section of the copper chamber using the He-Ne laser expanded into a sheet, the sheet must enter the chamber normal to the free surface. To illuminate a diameter using the He-Ne sheet and heat the surface in the center of the test cell using the CO_2 laser, the two laser beams must be in the same plane. A system was designed to eliminate blocking of either path by turning mirrors. Figures 10 and 11 show simplified front and top views of this design. The light sheet, created using plano-cylindrical lenses, is split into two sheets with prisms, allowing a section of the turning mirror, which reflects the sheet to the surface, to be removed. The two sheets are recombined as they converge on the test section. The CO_2 beam is reflected downward to the surface slightly above the He-Ne turning mirror, with the CO_2 beam passing through the cutout section of the He-Ne mirror, and with both beams in the same plane. A consequence of this design is the superposition of the two He-Ne sheets in the test cell. This creates a single sheet of nearly constant intensity, which eliminates the problem of nonuniform intensity caused by the Gaussian beam distribution. Figure 12 is an image created using the flow visualization system with a 35-mm SLR camera, utilizing streak photography, substituted for the SIT camera in order to illustrate the flow structure.

The flight versions of the He-Ne laser and intensified video camera (not necessarily an SIT camera) are the third and fourth major components that will be designed, fabricated, tested, and qualified for flight.

Postflight Data Analysis

The video record of the flow will be analyzed using a computerized particle image velocimetry (PIV) data reduction technique. Several systems are currently under investigation.[11-14] These systems track targets by following them from video frame to frame. After the images are digitized, the particles are outlined based on particle/background contrast. A centroid of the outline is the calculated, throwing out all other information. The centroids are then tracked though subsequent video frames. The frame acquisition rate is selectable to account for variations in flow velocity ranges throughout the test cross section. Although both systems accomplish the same end result, the tracking algorithms are significantly different producing data of different resolution and accuracy.

It has been demonstrated that one system[11,12] is able to track particles illuminated with a 5-mW He-Ne laser imaged with the SIT camera, and recorded using a standard VHS system and to produce quantitative data within the accuracies required by Ref. 8. This PIV data reduction technique is an ongoing activity, which is continuously being optimized to increase the resolution and accuracy of the reduced data.

Concluding Remarks

The laboratory components described herein along with the balance of the engineering model hardware presently being designed and fabricated at NASA Lewis, will constitute a working engineering model of the STDCE. For the flight hardware, the IR imager, CO_2 laser, He-Ne laser, and intensified video camera will be designed, fabricated, tested, and flight qualified by an outside source, and the balance of the flight hardware will be designed, fabricated, tested, and qualified at the NASA Lewis Research Center.

Acknowledgments

The authors would like to acknowledge and thank the members of the STDCE design team at the NASA Lewis Research Center for their involvement in and contributions to the design of these systems.

References

[1]Ostrach, S., "Low Gravity Fluid Flows," *Annual Review of Fluid Mechanics*, Vol. 14, 1982, pp. 313-345.

[2]Preisser, F., Schwabe, D., and Scharmann, A., "Steady and Oscillatory Thermocapillary Convection in Liquid Columns with Free Cylindrical Surface," *Journal of Fluid Mechanics*, Vol. 126, Jan. 1983, pp. 545-567.

[3]Kamotani, Y., and Ostrach, S., "Design of a Thermocapillary Flow Space Experiment," *Journal of Thermophysics and Heat Transfer*, Vol. 1, No. 1, 1987, pp. 83-89.

[4]Ostrach, S., Kamotani, Y., and Lai, C-L., "Oscillatory Thermocapillary Flow," *PCH Journal*, Vol. 6, No. 5/6, 1985, pp. 585-599.

[5]Napolitano, L. G., Monti, R., and Russo, G. "Some Results of the Marangoni Free Convection Experiment," *Proceedings of the 5th European Symposium on Material Sciences under Microgravity*, Schloss Elmau, FRG, Nov. 1984, pp. 15-22.

[6]Schwabe, D., Preisser, F., and Scharmann, A., "Verification of the Oscillatory State of Thermocapillary Convection in a Floating Zone Under Low Gravity," *Acta Astronautica*, Vol. 9, No. 4, 1982, pp. 265-273.

[7]Ostrach, S., "Convection Due to Surface Tension Gradients," *COSPAR Space Research*, Vol. 19, Pergamon, Oxford, England, 1979, pp. 563-570.

[8]Ostrach, S., and Kamotani, Y., "Science Requirements Document for the Surface Tension Driven Convection Experiment in Reduced Gravity," Case Western Reserve Univ., Cleveland, OH, 1987.

[9]Pline, A., "Infrared Surface Temperature Measurements for the Surface Tension Driven Convection Experiment," NASA TM 101353, 1988.

[10]Wenzler, C., and Echenberg, D., "Design of a CO_2 Laser Power Control System for a Spacelab Microgravity Experiment," NASA Lewis Research Center, Cleveland, OH (report in progress).

[11]Wernet, M. P., "Data Reduction Techniques for Pulsed Laser Velocimetery," Ph.D. Thesis, Case Western Reserve Univ., Cleveland, OH, 1988.

[12]Wernet, M. P., "A Vector Scanning Processing Technique for Pulsed Laser Velocimetry," *Proceedings of the 13th International Congress on Instrumentation in Aerospace Simulation Facilities (ICIASF)*, Institute of Electrical and Electronics Engineers, New York, 1989.

[13]Greaves, J. O. B., "State of the Art in Automated Motion Tracking and Analysis Systems," *Proceedings of the SPIE*, Bellingham, WA, Vol. 693, 1986, pp. 277-281.

[14]Walton, J. S., "The Accurcy and Precision of a Video-base Motion Analysis System," *Proceedings of the SPIE*, Bellingham, WA, Vol. 693, 1986.

Henry B. Garrett
Associate Editor